Structural Characterization of the Regulatory Proteins TenA and TenI from *Bacillus subtilis* and Identification of TenA as a Thiaminase II[†,‡]

Angela V. Toms, Amy L. Haas, Joo-Heon Park, Tadhg P. Begley,* and Steven E. Ealick*

Department of Chemistry and Chemical Biology, Cornell University, Ithaca, New York 14853

Received October 4, 2004; Revised Manuscript Received December 1, 2004

ABSTRACT: *Bacillus subtilis* gene products TenA and TenI have been implicated in regulating the production of extracellular proteases, but their role in the regulation process remains unclear. The structural characterization of these proteins was undertaken to help provide insight into their function. We have determined the structure of TenA alone and in complex with 4-amino-2-methyl-5-hydroxymethylpyrimidine, and we demonstrate that TenA is a thiaminase II. The TenA structure suggests that the degradation of thiamin by TenA likely proceeds via the same addition−elimination mechanism described for thiaminase I. Three active-site residues, Asp44, Cys135, and Glu205, are likely involved in substrate binding and catalysis based on the enzyme/product complex structure and the conservation of these residues within TenA sequences. We have also determined the structure of TenI. Although TenI shows significant structural homology to thiamin phosphate synthase, it has no known enzymatic function. The structure suggests that TenI is unable to bind thiamin phosphate, largely resulting from the presence of leucine at position 119, while the corresponding residue in thiamin phosphate synthase is glycine.

The biosynthesis of thiamin pyrophosphate has been the focus of considerable effort over the past decade; most of the proteins involved in assembly, salvage, transport, and degradation have now been identified and in many cases structurally and mechanistically characterized (*1*). A conspicuous exception is the TenA/TenI system.

In *Bacillis subtilis*, TenA and TenI are part of the thiazole biosynthetic operon (TenA−TenI−ThiO−ThiS−ThiG−ThiF−ThiD)[1] and both genes are known to be strongly repressed by thiamin (*2*). This suggests that TenA and TenI may have a role in thiamin biosynthesis or metabolism, but this potential role has to date remained unclear. However, it is known that TenA stimulates the production of degradative enzymes at the transcriptional level in *B. subtilis* and that this stimulation is attenuated by TenI (*3*). The production of the same degradative enzymes is also modulated by a class of proteins known as the Deg proteins (*4*). This observation suggests that there may be a relationship between TenA and TenI and the Deg proteins.

B. subtilis TenA is a 27 267 Da protein and is not essential for growth in thiamin-containing medium (*3*). TenA is widely distributed in eubacteria and archaea and its gene is usually found in a cluster with other thiamin biosynthetic and salvage genes. In bacteria, TenA is almost always found in a cluster with 4-amino-2-methyl-5-hydroxymethylpyrimidine/4-amino-2-methyl-5-hydroxymethylpyrimidine phosphate (HMP/HMP-P) kinase (ThiD), and in *Saccharomyces cerevisiae*, TenA and ThiD are fused (*5*). Efforts associated with structural genomics initiatives have led to the deposition in the Protein Data Bank of coordinates for TenA from *Pyrococcus furiosus* (PDB code 1RTW), *Pyrococcus horikoshii* (PDB code 1UDD), and *Bacillus subtilis* (PDB codes 1TYH and 1TO9). However, these studies did not provide insight into the function of TenA. The structure of the enzyme from *P. furiosus* indicated that TenA may bind HMP-P, one of the products of HMP/HMP-P kinase and a precursor to thiamin (PDB code 1RTW; unpublished results), based on the tentative assignment of electron density observed for a ligand that copurified with the protein.

B. subtilis TenI is a 22 783 Da protein and is also not essential for growth in thiamin-containing medium (*3*). TenI is less widely distributed than TenA and is usually found in a cluster of thiamin biosynthetic genes or with salvage genes with TenA (*5*). TenI shows significant sequence similarity to thiamin phosphate synthase (TPS; ThiE), particularly in the active-site region, suggesting that TenI may bind thiamin phosphate or one of the heterocyclic components of thiamin (*6*).

In this paper, we report the structure of TenA alone and in complex with HMP, and we demonstrate that TenA is a

[†] This work was supported by National Institutes of Health grant DK44083 (to T.P.B.). S.E.E. is indebted to the W. M. Keck Foundation and the Lucille P. Markey Charitable Trust.

[‡] The Protein Data Bank codes are 1YAF for TenA, 1YAK for the TenA complex with 4-amino-2-methyl-5-hydroxymethylpyrimidine, and 1YAD for TenI.

* To whom correspondence should be addressed at the Department of Chemistry and Chemical Biology, Cornell University, Ithaca, NY 14853. Telephone (607) 255-7961; fax (607) 255−1227; e-mail see3@cornell.edu or tbp2@cornell.edu.

[1] Abbreviations: HMP, 4-amino-2-methyl-5-hydroxymethylpyrimidine; HMP-P, 4-amino-2-methyl-5-hydroxymethylpyrimidine phosphate; ThiD, 4-amino-2-methyl-5-hydroxymethylpyrimidine/4-amino-2-methyl-5-hydroxymethylpyrimidine phosphate (HMP/HMP-P) kinase; TPS/ThiE, thiamin phosphate synthase; Thz-P, thiazole phosphate; IPTG, isopropyl β-D-thiogalactoside, SeMet, selenomethionine; thiamin-P, thiamin phosphate; APS, Advanced Photon Source; NCS, noncrystallographic symmetry; Thz, thiazole; TIM barrel, triosephosphate isomerase fold; thiamin-PP, thiamin pyrophosphate; HMP-PP, 4-amino-2-methyl-5-hydroxymethylpyrimidine pyrophosphate; FMOP, flavin mononucleotide-dependent oxidoreductase and phosphate binding.

10.1021/bi0478648 CCC: $30.25
Published on Web 01/28/2005

thiaminase II, an enzyme that degrades thiamin to its pyrimidine and thiazole components using water as a nucleophile. The thiaminase II activity had been previously described, but until now the gene encoding this enzyme was unknown. We also report the crystal structure of TenI and provide a model for the binding of thiazole phosphate (Thz-P) to TenI. The role of Thz-P binding by TenI is not yet understood.

EXPERIMENTAL PROCEDURES

Expression and Purification of TenA. B. subtilis TenA was subcloned into pDESTF1 (a Gateway-adapted vector based on the pET system from Novagen) and expressed in the BL21(DE3) strain of *Escherichia coli*. The native protein was obtained by inoculating 1 L of Luria−Bertani (LB) medium, supplemented with 100 μg/mL ampicillin, with a 10 mL saturated starter culture. The cells were grown at 37 °C until they reached an OD_{600} of ∼0.6, at which point they were induced with 1 mM isopropyl β-D-thiogalactoside (IPTG). After induction for 8 h, the cells were spun down and stored at −80 °C.

The cells were resuspended in binding buffer (50 mM NaH_2PO_4, pH 8.0, 300 mM NaCl, and 10 mM imidazole) and then lysed by sonication. The crude extract was centrifuged and the resulting supernatant was stirred for 1 h with 1.5 mL of Ni−NTA beads (Novagen) equilibrated with binding buffer. The resin was loaded onto a polypropylene column and washed with 5 column volumes of binding buffer followed by 50−100 column volumes of wash buffer (50 mM NaH_2PO_4, pH 8.0, 300 mM NaCl, and 20 mM imidazole). TenA was eluted from the column with elution buffer (50 mM NaH_2PO_4, pH 8.0, 300 mM NaCl, and 250 mM imidazole) and buffer-exchanged via gel filtration (Econo-Pac 10DG column, Bio-Rad) into the final storage buffer (20 mM Tris-HCl, pH 8.0). The protein was then concentrated to 12−18 mg/mL by use of a 10 kDa cutoff concentrator (Amicon) and stored at −80 °C. Protein concentrations were determined by the Bradford method (*7*) with bovine serum albumin as the standard. The purity of TenA was determined by Coomassie-stained SDS−PAGE analysis and was found to be greater than 99% (data not shown).

Expression and Purification of TenI. B. subtilis TenI was subcloned into pET-28a (named pBsTenI.28) and expressed in the BL21(DE3) strain of *E. coli* (Invitrogen). The native protein was obtained by inoculating 1 L of E salts minimal medium (0.8 mM $MgSO_4$, 10 mM citric acid, 72 mM K_2HPO_4, and 16 mM $Na_2NH_4PO_4{\cdot}2H_2O$) supplemented with 5 g/L dextrose and 35 μg/mL kanamycin with a 5 mL saturated starter culture. The cells were grown at 37 °C until they reached an OD_{600} of ∼0.6, at which point the temperature was lowered to 25 °C. The cells were induced with 500 μM IPTG. After induction for 6 h, the cells were spun down at 5000 rpm for 10 min and stored at −80 °C.

For production of selenomethionine- (SeMet-) incorporated protein, the methionine auxotrophic strain of *E. coli*, B834-(DE3) (Novagen), was transformed with pBsTenI.28 and the cells were grown under conditions slightly varied from those described above. The SeMet growth medium contained M9 salts supplemented with all amino acids (40 μg/mL each) except L-methionine, which was replaced with L-SeMet, 0.4% (w/v) glucose, 2 mM $MgSO_4$, 25 μg/mL $FeSO_4{\cdot}7H_2O$, 1 mM $CaCl_2$, 35 μg/mL kanamycin, and a 1% BME vitamin solution (Gibco−BRL). Cells from the initial 5 mL LB starter culture were washed with the SeMet-containing medium and used to start a 50 mL culture. This second culture was grown to an OD_{600} of ∼0.6 and used to inoculate a 1 L culture. The rest of the expression was performed as described above.

All purification steps were carried out at 4 °C and all purification buffers for TenI were augmented with 1 mM thiamin phosphate (thiamin-P). Cells were resuspended in binding buffer and then lysed by sonication. The crude extract was centrifuged and the resulting supernatant was stirred for 1 h with 1.5 mL of Ni−NTA beads (Novagen) equilibrated with the binding buffer. The resin was loaded onto a polypropylene column and washed with 100 mL of binding buffer followed by 50 mL of wash buffer. TenI was eluted from the column with 15 mL of elution buffer. The eluted protein was buffer exchanged via gel filtration (Econo-Pac 10DG column, Bio-Rad) into the final storage buffer (25 mM Tris-HCl, pH 8.5, 150 mM NaCl, and 1 mM thiamin-P). The protein was then concentrated to 10−12 mg/mL using a 10 kDa cutoff concentrator (Amicon) and stored at −80 °C. Protein concentrations were determined by the Bradford method (*7*) with bovine serum albumin as the standard. The purity of TenI was determined by Coomassie-stained SDS−PAGE analysis and found to be greater than 99% (data not shown).

Crystallization of TenA. Small initial crystals of TenA were obtained by use of the Crystal Screen sparse matrix kit (Hampton Research; *8*). Crystallization trials were carried out at room temperature by the hanging drop method by mixing 1 μL of well buffer with 1 μL of protein solution. TenA was diluted to 10−12 mg/mL for all crystallization trials. The well solution for the crystallization of TenA contained 26% 2-methyl-2,4-pentanediol with 0.1 M sodium citrate, pH 4.4, and 20 mM $MgCl_2$. Crystals appeared overnight and took 1−2 weeks to reach their maximum size of 0.1 mm × 0.1 mm × 0.15 mm. These crystals were flash-frozen in liquid nitrogen directly from the droplet and stored for later use. The crystals belong to the orthorhombic space group $P2_12_12_1$, with $a = 58.43$ Å, $b = 58.26$ Å, and $c = 297.02$ Å. The asymmetric unit contains four TenA monomers, corresponding to a solvent content of 45%.

It was not possible to obtain cocrystals of TenA with HMP under these crystallization conditions, and crystals of TenA grown in the absence of HMP cracked almost immediately when exposed to very low HMP concentrations. To obtain crystals of TenA complexed with HMP, new crystallization conditions were required. Alternate crystallization conditions for the TenA−HMP complex were obtained by use of the Crystal Screen II sparse matrix kit (Hampton Research). For cocrystallization of TenA with HMP, the protein solution was preincubated with 1 mM HMP for 3 h prior to crystallization. The optimized well solution contained 0.7 M 1,6-hexanediol with 0.1 M sodium acetate, pH 4.4, and 10 mM $MgCl_2$. Crystals appeared in 1−2 days and took 1−2 weeks to reach their maximum size of 0.4 mm × 0.08 mm × 0.05 mm. For cryoprotection, the TenA−HMP cocrystals were briefly transferred into a cryoprotection buffer containing 0.73 M 1,6-hexanediol, 0.1 M sodium acetate, pH 4.4, 10 mM $MgCl_2$, 2.2 mM HMP, and 14% glycerol. The

crystals were frozen directly in the cryostream immediately prior to data collection. X-ray analysis indicated that the crystals belonged to space group $C222_1$, with $a = 82.96$ Å, $b = 82.93$ Å, and $c = 296.36$ Å. There are four TenA monomers in the asymmetric unit, corresponding to a solvent content of 46%.

Crystallization of TenI. Small initial crystals of TenI were also obtained by use of the Crystal Screen sparse matrix kit (Hampton Research; *8*). Crystallization trials were carried out at room temperature by the hanging drop method by mixing 2 μL of well buffer with 1 μL of protein solution. The well solution for optimized conditions for both the native and SeMet-TenI contained 2.0−2.3 M ammonium sulfate with 0.1 M bicine, pH 9.0, 2% poly(ethylene glycol) 400, and 5−10 mM L-cysteine. Crystals took 5−7 days to appear and 4−6 weeks to reach their maximum size of 0.2 mm × 0.05 mm × 0.05 mm. For cryoprotection, the TenI crystals were briefly transferred into a cryoprotection buffer similar to the mother liquor but with the ammonium sulfate concentration increased by 100 mM relative to the mother liquor and 20% glycerol added. The crystals were flash-frozen by plunging them into liquid nitrogen and stored for later use. Preliminary X-ray analysis showed that the crystals belonged to space group $C222_1$, with $a = 96.97$ Å, $b = 104.24$ Å, and $c = 217.35$ Å. Each asymmetric unit contains four TenI monomers, corresponding to a solvent content of 57%.

X-ray Data Collection and Processing. The native TenA X-ray intensity data were measured at the NE-CAT beamline 8-BM of the Advanced Photon Source (APS) by use of a Quantum 315 detector (Area Detector Systems Corp.). The data set was collected over a range of 100° by use of 20 s for each 0.5° oscillation at a crystal to detector distance of 400 mm. The TenA−HMP complex data was collected at the F2 station of the Cornell High Energy Synchrotron Source (CHESS) using a Quantum 210 detector (Area Detector Systems Corp.). The data were collected over a range of 105° using 60 s for each 0.5° oscillation at a crystal to detector distance of 290 mm.

All TenI data were measured at the NE-CAT beamline 8-BM at APS by use of a Quantum 315 detector (Area Detector Systems Corp.). A single-wavelength anomalous data set was collected to 2.5 Å resolution. Following calibration of the beam with a Se foil, a fluorescence scan was taken on a SeMet-TenI crystal. For data collection, the wavelength corresponding to the maximum of f'' (peak) was chosen. Due to crystal decay problems only a single wavelength could be collected. Data were collected over a range of 120° by use of 30 s for each 1.0° oscillation at a crystal to detector distance of 300 mm. Bijvöet pairs were measured after each 10° wedge by inverse beam geometry. A native data set was collected over a range of 140° by use of 10 s for each 1° oscillation at a crystal to detector distance of 270 mm.

The HKL2000 suite (*9*) of programs was used for integration and scaling of all data sets. The data collection statistics are summarized in Table 1.

Phasing, Model Building, and Refinement of TenA. The structures of TenA from *P. horikoshii* and *P. furiosus* (PDB codes 1UDD and 1RTW) (*10*) served as templates for generating a homology model of BsTenA by use of MODELLER (*11*, *12*). The homology model of the BsTenA monomer was then utilized as the search model for molecular replacement with MOLREP (*13*, *14*). The final solution had a crystallographic *R*-factor of 49.2% for data from 15 to 3 Å. All model building was preformed with the computer program O (*15*). The refinement procedure was carried out by Crystallography & NMR System (CNS; *16*) and consisted of successive rounds of rigid-body refinement, simulated annealing, temperature factor refinement, and model rebuilding. In the native structure, some electron density for which we cannot account was observed connecting residues Asp44, Cys135, and Glu205 and was modeled as a series of water molecules. The final refinement statistics are shown in Table 2. Figures were prepared by use of Molscript (*17*, *18*), Bobscript (*17*), Raster3D (*19*), and Spock (*20*).

SAD Phasing of TenI. The initial Se atom positions were determined by shake-and-bake direct methods (*21*) as implemented in SnB (*22*). The peak wavelength data to 3.0

Table 1: Data Collection and Processing Statistics

	SeMet−TenI peak	TenI native	TenA native	TenA complex
space group	$C222_1$	$C222_1$	$P2_12_12_1$	$C222_1$
cell dimensions (Å)	$a = 96.97$	$a = 96.84$	$a = 58.43$	$a = 82.96$
	$b = 104.24$	$b = 103.78$	$b = 58.26$	$b = 82.93$
	$c = 217.35$	$c = 217.05$	$c = 297.02$	$c = 296.36$
wavelength (Å)	0.9791	0.9791	0.9795	0.9795
resolution (Å)	2.5	2.1	2.6	2.5
mosaicity (deg)	0.29	0.20	0.28	0.54
no. of reflns	333 702	418 985	87 145	131 908
no. of unique reflns	65 257	72 558	30 807	33 460
redundancy[a]	4.9 (4.8)	5.8 (5.8)	2.8 (2.8)	3.9 (2.6)
completeness[a] (%)	79.2 (83.9)	98.5 (98.1)	95.5 (90.1)	93.4 (66.2)
R_{sym}[a,b] (%)	11.5 (26.4)	8.8 (39.6)	8.8 (21.6)	6.3 (26.4)
I/σ_I[a]	13.3 (4.3)	18.8 (4.3)	13.3 (6.85)	21.3 (3.2)

[a] Values for the outer resolution shell (2.59−2.5 and 2.15−2.07 Å for the peak and native TenI data sets, respectively and 2.7−2.6 and 2.59−2.5 Å for the TenA native and complex data sets, respectively) are given in parentheses. [b] $R_{sym} = \Sigma\Sigma_i|I_i - \langle I\rangle|/\Sigma\langle I\rangle$, where $\langle I\rangle$ is the mean intensity of N reflections with intensities I_i and common indices h, k, and l.

Table 2: Refinement Statistics and Model Building

	TenI	TenA	TenA−HMP
resolution (Å)	2.1	2.6	2.5
total no. of non-hydrogen atoms	6509	7335	7464
no. of protein atoms	5902	7204	7234
no. of water oxygen atoms	543	131	190
no. of reflns in refinement	61 326	28 907	31 736
no. of reflns in the test set	3117	1508	1681
R-factor[a] (%)	19.6	24.0	21.7
R_{free}[b] (%)	22.1	28.6	25.5
rms deviation from ideal geometry			
bonds (Å)	0.005	0.007	0.008
angles (deg.)	1.3	1.1	1.2
Ramachandran plot			
most favored (%)	91.6	93.6	91.0
allowed (%)	8.1	5.1	9.0
generously allowed (%)	0.3	0.8	0.0
disallowed (%)	0.0	0.0	0.0
average *B*-factors (Å)^2			
main chain	23.6	42.5	60.9
side chain	27.5	49.6	66.6
solvent	37.4	41.9	67.8
ligand	31.9		55.2

[a] R factor $= \Sigma_{hkl}||F_{obs}| - k|F_{calc}||/\Sigma_{hkl}|F_{obs}|$, where F_{obs} and F_{calc} are the observed and calculated structure factors, respectively. [b] For R_{free}, the sum is extended over a subset of reflections (5%) excluded from all stages of refinement.

Å were used to calculate normalized anomalous differences (ΔE) by use of the DREAR (*23*) suite of programs. A total of 800 ΔE values with $\Delta E/\sigma$ (ΔE) values of >3.0 and 8000 triplet invariants were used to carry out 370 random trials with 150 cycles of phase refinement per trial. Twelve of these trials produced solutions as judged by the behavior of the shake-and-bake minimal function. From these phases, 16 of the possible 20 Se atom positions were identified. The Se atom positions were input into CNS (*16*) and used for phasing. The initial phases were used to identify the four remaining Se atom positions from a combination of anomalous difference Fourier and log-likelihood Fourier maps, and the phases were recalculated with the 20 Se atom positions. The selenium sites were divided into two sets of 10 atoms, each exhibiting a noncrystallographic symmetry (NCS) 2-fold axis.

Model Building and Structure Refinement of TenI. All model building was performed with the computer program O (*15*). Electron density maps were calculated and improved by use of both NCS constraints and solvent flattening. The protein mask for solvent flattening was created from the superposition of the thiamin phosphate synthase (PDB code 2TPS) structure with the initial electron density map. An initial model, consisting of most of the residues between Met1 and Lys197, was built and the other monomers were generated with NCS. At this stage, residues 125−135 and eight C-terminal residues were omitted from the model due to poor electron density in those regions. Several amino acid residues, including Arg18, Arg35, Lys37, Glu51, Lys86, Arg146, and Asp160, were truncated to alanine. The refinement procedure consisted of successive rounds of rigid-body refinement, simulated annealing refinement with NCS restraints, temperature factor refinement, and model rebuilding. In the latter stages of model building, the higher resolution native data were utilized. The final refinement statistics are shown in Table 2. Figures were prepared by use of Molscript (*17*, *18*), Bobscript (*17*), and Raster3D (*19*).

Modeling of Thiazole Phosphate into the Active Site of TenI. Thiazole phosphate was modeled into the active site of TenI with the program O (*15*). The TPS/thiamin-P complex (PDB code 1G4S) was superimposed on the TenI structure and the thiamin-P molecule was used as a template to model Thz-P. The position of the observed crystallographic sulfate ion in the TenI structure was also used as a basis for positioning the phosphate moiety of Thz-P.

Identification of TenA Catalytic Activity in the Degradation of Thiamin. The thiaminase activity of TenA was identified by incubating TenA (25 μM), and thiamin (2.5 mM) at room temperature in 50 mM Tris, pH 8.0. A 100 μL aliquot of this reaction mixture was removed after 1 min, quenched by heating at 95 °C for 5 min, and analyzed by HPLC on a C_{18} column (Supelco, Supelcosil LC-18-T 15 cm × 4.6 cm, 3 μm) equilibrated with 100 mM phosphate buffer at pH 6.6 at a flow rate of 1 mL/min. HMP, thiamin, and the thiazole (Thz) were detected by absorbance at 254 nm and eluted at 12, 14, and 24 min, respectively, with a methanol gradient of 0% (0−4 min), 5% (4−15 min), 30% (15−20 min), and 0% (20−22 min). The chromatogram of this reaction is shown in Figure 1A and indicates that, in the presence of TenA, thiamin is rapidly degraded to HMP and Thz. Product identification was also confirmed by NMR analysis (data not shown). TenA specifically catalyzes the cleavage of thiamin; thiamin-P and thiamin pyrophosphate (thiamin-PP) are not substrates.

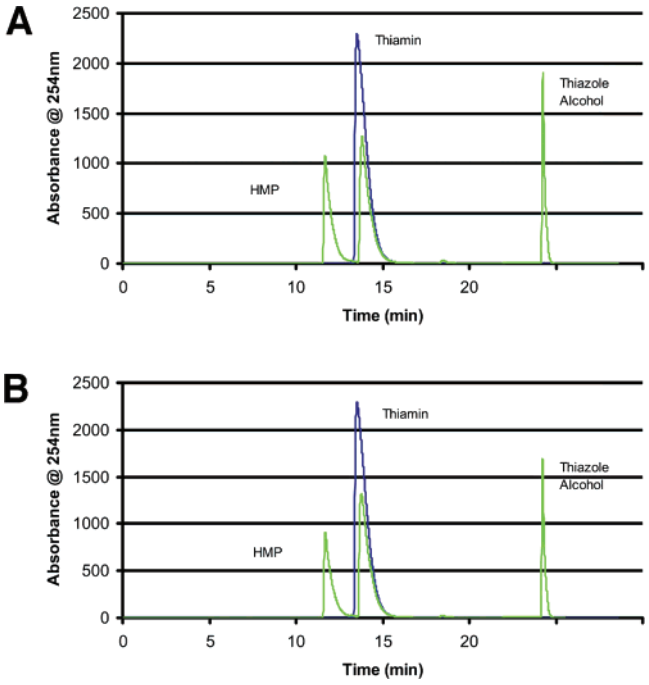

FIGURE 1: Thiaminase activity of TenA. (A) HPLC analysis of the TenA-catalyzed degradation of thiamin. The blue trace is of the control reaction with no TenA, and the green trace is of the TenA reaction. (B) HPLC analysis of the TenA-catalyzed degradation of thiamin in the presence of TenI. The blue trace is of the control reaction with no TenA or TenI, and the green trace is of the TenA- and TenI-containing reaction.

Investigation of the Effect of TenI on the Activity of TenA. To determine if TenI directly modulates the thiaminase activity of TenA, the thiaminase reaction was run as described above but in the presence and absence of TenI (25 μM). The results of the HPLC analysis of this reaction are shown in Figure 1B and demonstrate that TenI does not inhibit or activate the thiaminase activity of TenA. The TenA/TenI reaction was also run in the presence of Thz (2.5 mM) or Thz-P (2.5 mM). Again, no effect on the TenA activity was detected.

RESULTS

Overall TenA Structure. We have determined the crystal structures of unliganded BsTenA and the BsTenA complex with HMP. The current models consists of 7204 non-hydrogen protein atoms and 131 water molecules for the unliganded protein and 7234 non-hydrogen protein atoms, 40 non-hydrogen ligand atoms, and 190 water molecules for the HMP complex structure. The TenA monomer has a roughly rectangular box shape with dimensions of 46 Å × 30 Å × 25 Å. The TenA fold is a single domain, all-α-helical protein consisting of 11 α-helices (Figure 2). A deep acidic pocket is located in the central region of the protein surrounded by helices α4, α5, α9, and α10 (Figure 2C). The pocket is lined with a large number of aromatic and acidic residues and has a volume of approximately 700 Å^3.

TenA Quaternary Structure. TenA is a tetramer with 222 point symmetry and has a rectangular box shape with dimensions 70 Å × 65 Å × 45 Å (Figure 2D). In the unliganded TenA structure, the four monomers of the

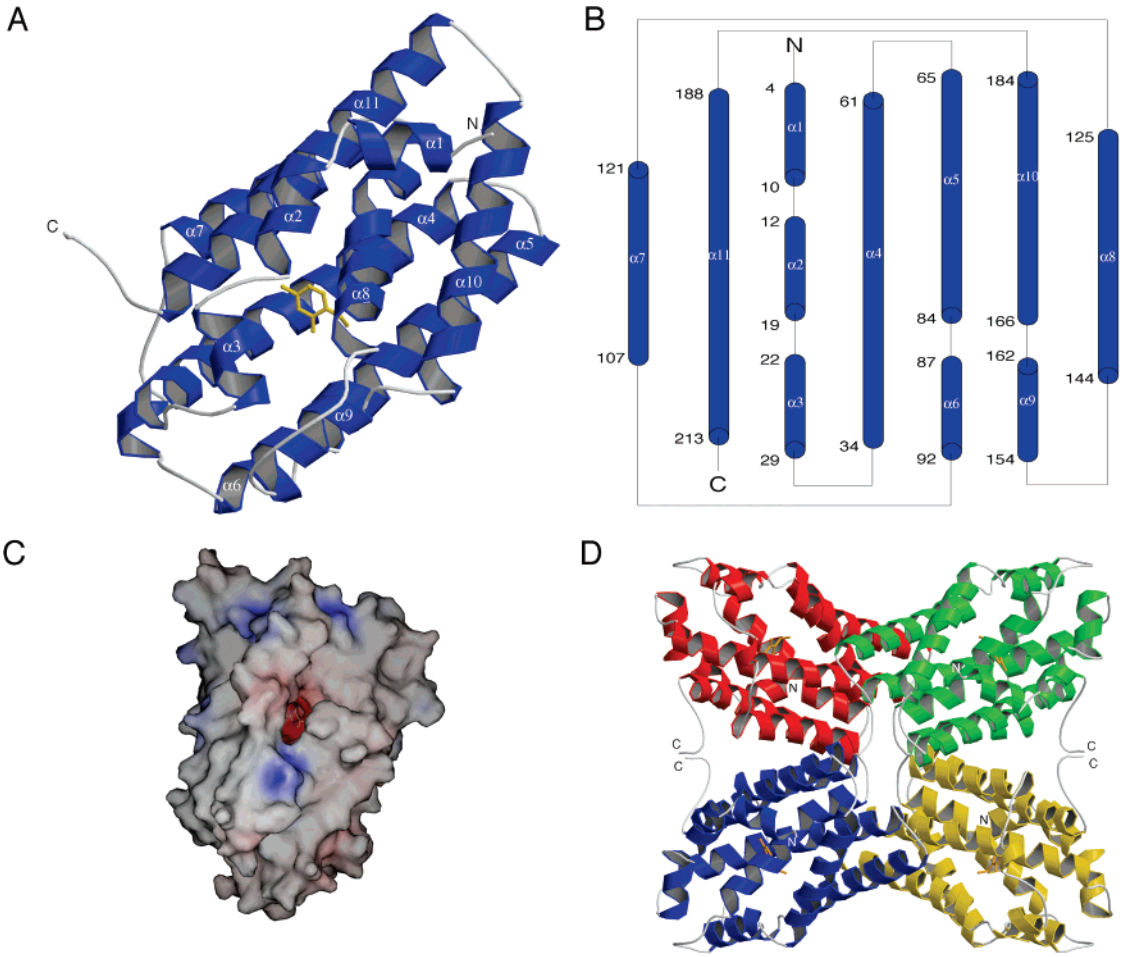

FIGURE 2: Structure and topology of TenA. (A) Ribbon diagram of the TenA monomer. The secondary structural elements are labeled sequentially α1−α11 on the basis of their positions in the sequence. HMP is shown bound to the monomer in stick representation. (B) Topology diagram for TenA. The secondary structural elements are labeled, and the first and last residues for each are numbered. (C) Electrostatic surface representation of TenA. Only protein atoms were considered for the surface calculation. The surface is colored blue for positively charged areas, red for negatively charged areas, and gray for neutral areas. (D) Structure of the TenA tetramer. Each monomer is shown in a different color. HMP is shown bound to each monomer in orange.

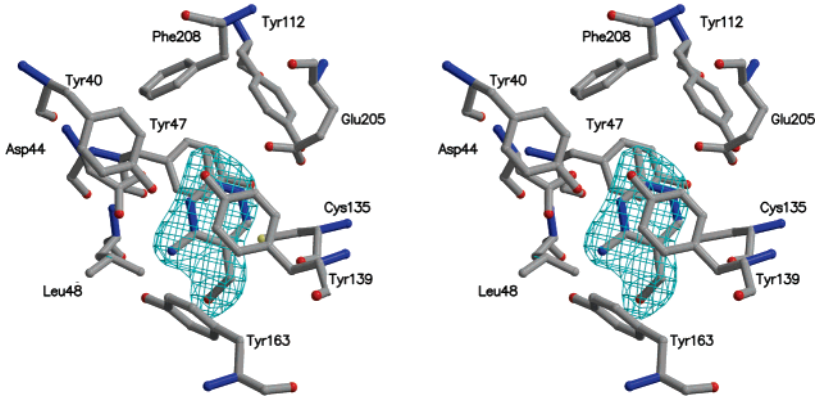

FIGURE 3: Stereoview of an $F_{obs} - F_{calc}$ electron density map for the HMP binding site of TenA contoured at 4σ. For the calculation of the map, the HMP molecule was omitted from the model. The TenA residues are shown in ball-and-stick representations with oxygen atoms in red, carbon in gray, nitrogen in blue, and sulfur in yellow.

tetramer are related by three mutually perpendicular non-crystallographic 2-fold axes. Each monomer makes contacts with two other monomers. The main interactions between monomers A and D are through helices α7 and α11. In the interface, both hydrophobic and hydrogen-bonding interactions are observed. The A−D interface buries a total surface area of 2156 Å^2. The interface between monomers A and C involves the antiparallel stacking of helices α4 and α5 from both monomers. This interface contains more hydrophobic interactions than the A−D interface but also contains hydrogen bonds. The A−C interface buries a total surface area of 1780 Å^2.

TenA HMP Binding Site. The electron density for crystals grown in the presence of HMP clearly showed one HMP molecule per monomer (Figure 3). The HMP molecule is bound deep within the acidic pocket. The pyrimidine ring

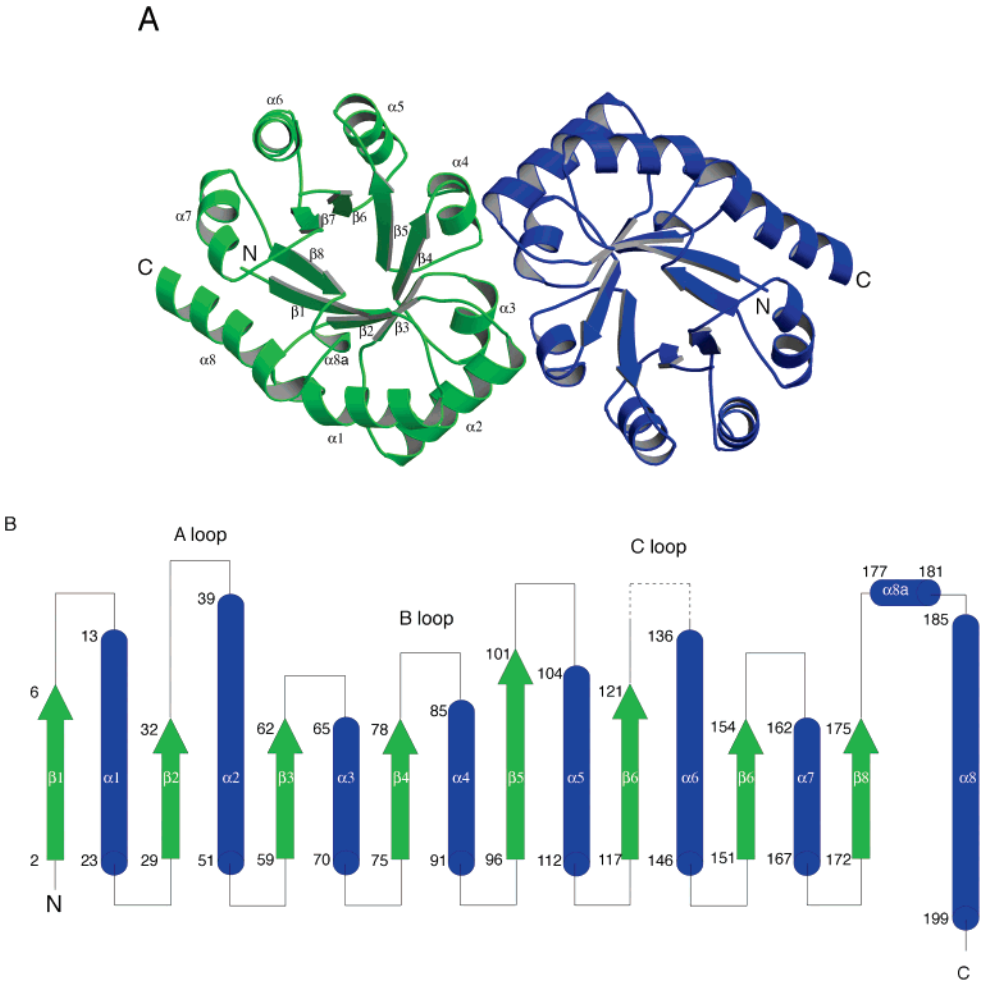

FIGURE 4: Structure and topology of TenI. (A) Ribbon diagram of the TenI dimer. The structural elements for one monomer are labeled sequentially α1−α8 and β1−β8 on the basis of the convention for $(\beta\alpha)_8$ TIM barrels, with the additional helix between β7 and α8 labeled as α8a. (B) Topology diagram for TenI. The secondary structural elements are labeled, and the first and last residues for each are numbered.

of the HMP molecule is sandwiched between two tyrosine residues (Tyr47 and Tyr139), with a ring stacking distance of 3.56 Å. The binding of HMP is also stabilized by a number of electrostatic and hydrogen-bonding interactions. The 4-amino group and the N3 nitrogen atom of the pyrimidine ring both form hydrogen bonds with Asp44. The N1 atom of HMP is in close proximity to Glu205. The sulfur atom of Cys135 is located about 3 Å from the C6 position of the pyrimidine ring.

Identification of TenA Activity. In an attempt to identify a small molecule, related to thiamin biosynthesis, that binds to TenA or TenI, we incubated TenA, TenI, and both TenA and TenI together with HMP, HMP-P, HMP-PP, Thz, Thz-P, thiamin, thiamin-P, and thiamin-PP. The experiment was performed with all small molecules and proteins in a 1:1 molar ratio. The putative small molecule−protein complex was removed by rapid gel filtration and the remaining small molecule pool was analyzed for depletion of one or more of its components by NMR and HPLC. TenA showed an affinity for HMP, but we were unable to detect any small molecules binding to TenI. Most significantly, these experiments revealed that TenA selectively degraded thiamin to HMP and Thz (Figure 1). TenI did not modulate the catalytic activity of TenA.

Quality of the TenI Model. The asymmetric unit contains four monomers of TenI (labeled A−D), eight sulfate ions, and a total of 543 water molecules. The four monomers are organized into two independent dimers. Monomers A, C, and D include residues 1−124 and 135−200; monomer B consists of residues 1−124 and 132−200. A total of 21 residues showed disordered side chains and were modeled as alanine. These residues include Lys86 and Arg163 in monomers A−D; Arg135 in monomers A, C, and D; Lys166 in monomers A−C; Arg200 in monomers C and D; Asp160 in monomer A; Lys44 in monomer B; and Arg146 and Lys197 in monomer C. There were no cis-peptide bonds, and no disulfide bonds were observed. The final model was assessed with the programs PROCHECK (*24*) and O (*15*). The structure refined to a final *R* factor of 19.6%, with an R_{free} of 22.1%. The Ramachandran plot (*25*) showed that 91.6% of the main-chain dihedral angles lie in the most favorable region and 8.1% are found in the additional favored region. The average *B*-factor is 23.6 Å^2 for main-chain atoms, 27.5 Å^2 for side-chain atoms, and 37.4 Å^2 for water molecules. The *B*-factors for the sulfate ions range from 26.6 to 39.4 Å^2.

TenI Architecture and Topology. The TenI momoner has a $(\beta\alpha)_8$ barrel fold. The overall dimensions are approximately 45 × 45 × 30 Å^3. The eight parallel β-strands, which are tilted approximately 45° from the axis of the barrel as expected, and eight surrounding helices (α1−α8) are shown in Figure 4. There is one additional α-helix, α8a, which

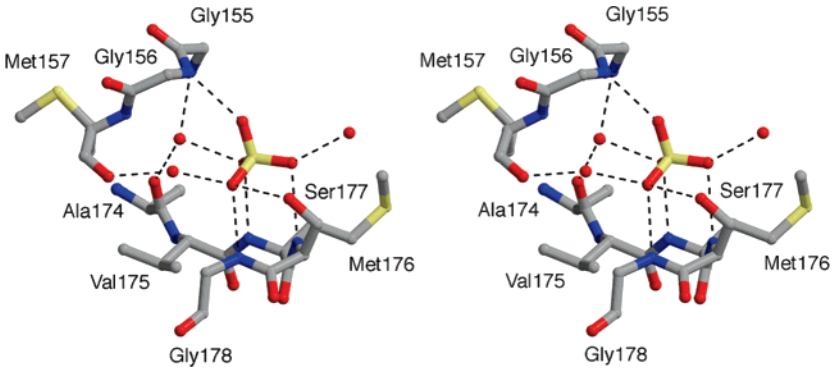

FIGURE 5: Stereo diagram of the TenI sulfate binding site. Hydrogen bonds are indicated by dashed lines. The water molecules are shown as red spheres. The TenI residues are shown in ball-and-stick representations with the atoms colored according to the scheme described for Figure 3.

consists of a single turn. The α8a helix is situated between β7 and α8 and is tilted approximately 20° from the axis of the TIM barrel. The majority of the β-strands consists of four amino acid residues except for β1, β5, and β6, which consist of five, six, and five amino acid residues, respectively. The lengths of the helices range from 4 to 15 residues long, with α8a being the shortest and α8 the longest. TenI contains a mainly hydrophobic core formed by residues from the β-strands that point into the interior of the barrel.

TenI Dimer Interactions. The TenI crystal structure contains two $(\beta\alpha)_8$ barrel dimers, with the barrel axes for each dimer oriented approximately parallel to each other (Figure 4). Monomers A and B are related by one NCS 2-fold axis and monomers C and D are related by a second NCS 2-fold axis. The total surface area buried at the dimer interface is 1560 and 1490 Å^2 for the A−B and C−D interfaces, respectively. The main interactions between monomers A and B (also for C and D) are hydrophobic contacts involving C-terminal loops of β2, β3, and β4, as well as contacts between the helices α3 and α4. Helix α3 of one monomer is oriented roughly perpendicular to the barrel axis of the other monomer, forming primarily hydrophobic interactions with α3 and α4. A single intermolecular hydrogen bond is observed in this region between Asp66 and the backbone amide nitrogen of Leu65′ (the primed residues refer to residues in the 2-fold related monomers).

TenI Crystal Packing. The interface between the A−B dimer with the C monomer of the second dimer is dominated by water-mediated hydrogen bonds between the N-terminal loops of β5 from both the A and B monomers with α6 and α7 of the C monomer. The contact surface between the two dimers is 1040 Å^2. The dimer-to-dimer contacts are likely an artifact of crystal packing.

TenI Sulfate Binding Sites. Clear electron density for a sulfate ion is observed at the N-terminus of α8a in each monomer. The sulfate ion forms hydrogen-bonding interactions with Met176 (N), Ser177 (N and Oγ), and Gly178 (N) and also contacts the β7−α7 loop through a hydrogen bond to Gly156 (N). Of these residues Gly156, Gly178, and Ser177 are conserved in all TenI sequences. The sulfate ion is further stabilized by hydrogen-bonding interactions with three water molecules (Figure 5).

DISCUSSION

Structural Similarity of TenA to Other Proteins. The TenA monomer was submitted to the DALI server (*26*) to identify other proteins of similar structure. The search revealed that the BsTenA structure had recently been solved by two structural genomics groups (PDB codes 1TYH and 1TO9). The structures of TenA from *B. subtilis*, *P. horikoshii*, and *P. furiosus* all exhibit a very similar fold, with a deep acidic binding pocket. As previously noted (*10*), TenA also bears a structural resemblance to heme oxygenase 1 (HO-1) proteins.

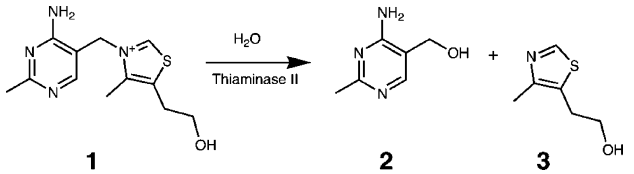

FIGURE 6: Thiaminase II-catalyzed hydrolysis of thiamin.

Identification of TenA as Thiaminase II. Thiaminases catalyze the degradation of thiamin. This activity has been detected in bacteria, marine organisms, and plants (*27*, *28*). Two classes of thiamin-degrading enzymes have been identified. Thiaminase I (EC 2.5.1.2) catalyzes the reaction in which the thiazole group of thiamin is replaced by a variety of organic nucleophiles. Thiaminase I from *Bacillus thiaminolyticus* has been biochemically and structurally characterized (*29*−*32*). Thiaminase II is specific for the use of water as the nucleophile and the cleavage of thiamin yields HMP and Thz (Figure 6). Thiaminase II activity has been detected in *Bacillus thiaminolyticus*, *Clostridium*, *Oospora lactis*, *Saccharomyces cerevisiae*, *Trichosporon aneurinolyticum*, *Bacillus aneurinolyticus*, and *Candida aneurinolytica*, but its gene has not previously been identified. The studies reported here demonstrate that TenA is responsible for the thiaminase II activity in *B. subtilis*.

Catalytic Mechanism of TenA. The mechanism of thiaminase I is now well understood and is outlined in Figure 7. Addition of the thiol of Cys113 to C6 of the pyrimidine gives carbanion **5**, which drives the elimination of the thiazole. Addition of the thiamin-cleaving nucleophile to **7** followed by elimination of the cysteine thiolate completes the thiamin cleavage reaction. Direct displacement of the thiazole of thiamin is without precedent in thiamin chemistry, and the addition−elimination mechanism described in Figure 7 is the only known way to carry out this reaction (*33*). One might therefore anticipate that while the sequence and structures of thiaminase I and TenA (thiaminase II) are very different, a similar catalytic functionality would be used by both enzymes.

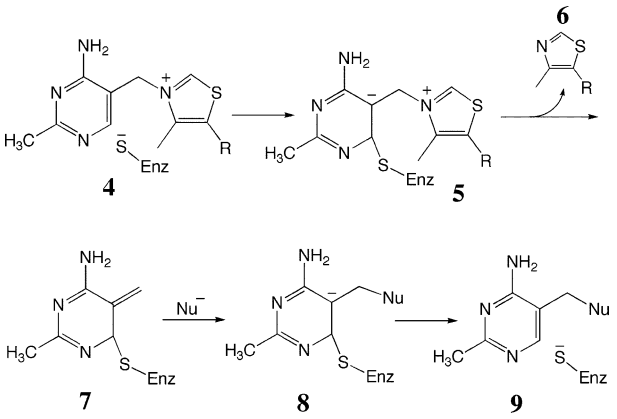

FIGURE 7: Proposed catalytic mechanism of thiaminase I and thiaminase II (TenA).

The active sites of thiaminases I and II are shown in Figure 8. In TenA the electrophilicity of the pyrimidine is enhanced by hydrogen bonding of N1 and N3 to Glu205 and Asp44, respectively, and the thiol of Cys135 is suitably positioned to add to C6 of the pyrimidine. While there is no basic residue close to Cys135 to assist deprotonation, the electropositive active-site environment may be sufficient to lower the cysteine pK_a. In addition, a hydrogen-bonding network exists between the N1 nitrogen atom of HMP and the Sγ atom of Cys135 (through the side chains of residues Glu205, Tyr112, and Tyr47). The Sγ atom of Cys135 is 3 Å from the hydroxyl group of Tyr47, which is 3.2 Å from the hydroxyl group of Tyr112. The hydroxyl group of Tyr112 shows a strong hydrogen bond to the Oδ1 atom of Glu205, with a separation distance of 2.6 Å. The Oδ2 atom of Glu205 is then hydrogen-bonded to the N1 nitrogen atom of HMP, completing the hydrogen-bonding network. This network may serve as a proton shuttle to deprotonate Cys135 and protonate the N1 atom of HMP (Figure 8). In thiaminase I, the active-site cysteine is activated by Glu241 and can be labeled with a mechanism-based inactivating thiamin analogue. This complicates the assignment of function to the active-site residues because the inactivation mechanism involved the rearomatization of the initially formed pyrimidine thiol adduct, which distorts the position of the pyrimidine at the active site and breaks the hydrogen bond between N3 of the pyrimidine and Asp272. The major difference between thiaminase I and thiaminase II resides in the nature of the cleaving nucleophile. Thiaminase I uses a wide variety of nucleophiles (aniline, quinoline, cysteine, pyridoxol), while thiaminase II is specific for water. This is consistent with the structural analysis, which shows that the thiaminase I active site is open while the TenA active site is buried with only a small volume accessible to the nucleophile.

Comparison of TenI to Related Proteins. A structural search with DALI (*26*) showed that the top 20 structural alignments to TenI are dominated by proteins from the FMOP superfamily. The FMOP superfamily is characterized by a conserved phosphate binding pocket consisting of residues from β6, β7, and α8a. The top alignment of TenI was to the *B. subtilis* thiamin phosphate synthase. TenI also aligns well with the $(\beta\alpha)_8$ domain of pyruvate kinase (PDB code 1A49) from rabbit muscle (*34*). Pyruvate kinase adopts a $(\beta\alpha)_8$ structure with an additional domain inserted at the

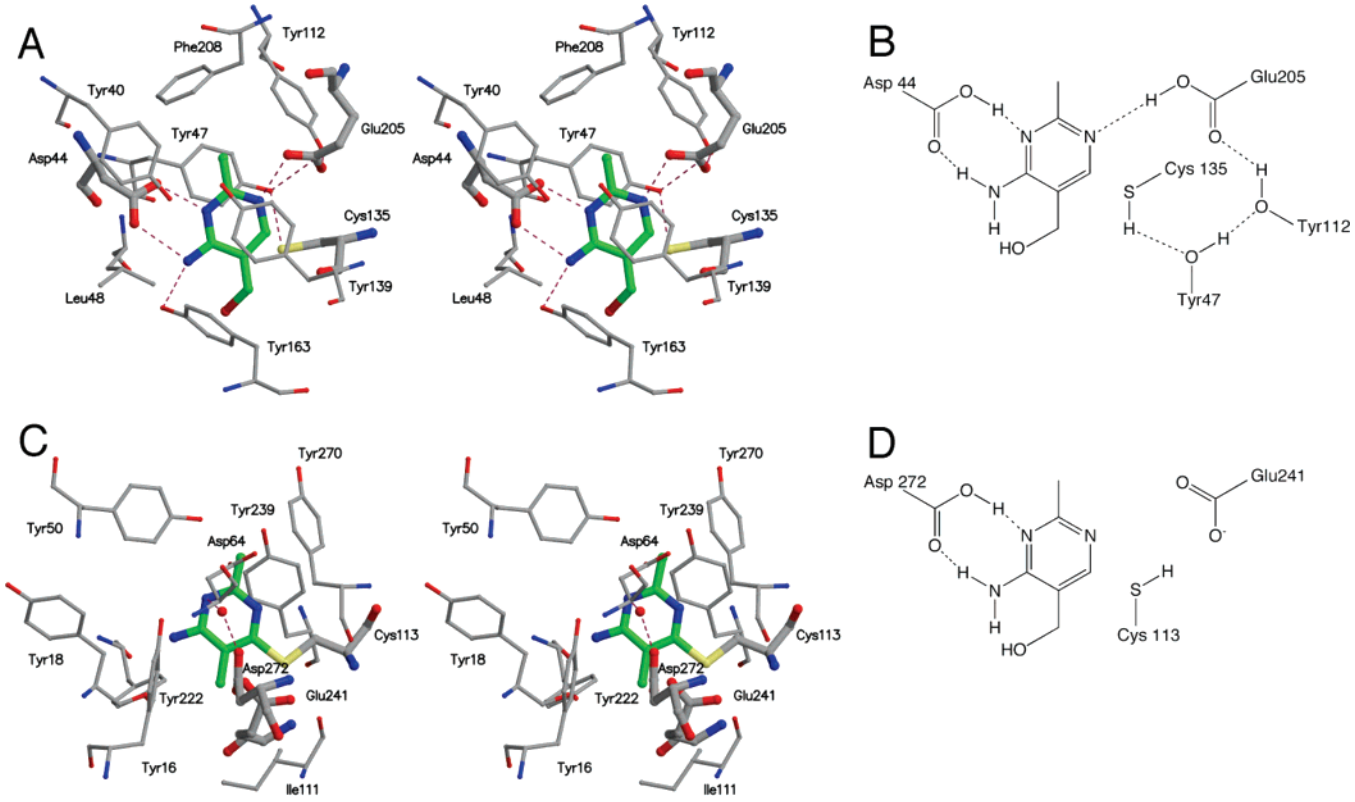

FIGURE 8: Comparison of the active sites of TenA and thiaminase I. (A) Stereodiagram of the TenA active site with HMP bound. (B) Schematic of the key TenA active-site interactions with HMP. (C) Stereodiagram of the thiaminase I active site with the covalently bound 4-amino-6-chloro-2,5-dimethylpyrimidine inhibitor. (D) Schematic of the key thiaminase I active-site interactions with HMP derived from the structure of the inhibited enzyme shown in panel C. Hydrogen bonds are indicated by dashed lines. The residues are shown in ball-and-stick representations with the atoms colored according to the scheme described for Figure 3. The bound ligand molecule is highlighted in green.

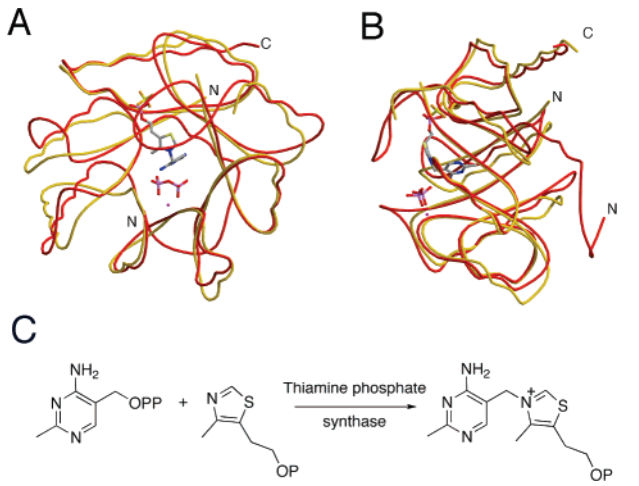

FIGURE 9: Superposition of TenI with TPS (PDB code 2TPS). (A) View looking down the barrel. (B) Side view perpendicular to the barrel axis. Shown in ball-and-stick representation are the thiamin phosphate, pyrophosphate, and Mg^{2+} observed in the TPS crystal structure and the sulfate ion observed in the TenI structure. The oxygen atoms for the TenI sulfate ion are shown in orange; the other atoms are colored according to the scheme described for Figure 3. (C) TPS-catalyzed formation of thiamin phosphate.

end of β3 and a further domain at the C-terminus of the barrel. The enzyme binds ATP, phosphoenolpyruvate, and Mg^{2+}. While pyruvate kinase does not contain the conserved phosphate binding site found in TenI and other members of the FMOP superfamily, the conformation of the protein backbone in β7 and the following loop is similar to that observed for the FMOP superfamily.

Comparison of TenI to Thiamin Phosphate Synthase. Thiamin phosphate synthase catalyzes the formation of thiamin-P from Thz-P and HMP-PP (*6*). The structures of wild-type and mutant TPS from *B. subtilis* have been previously determined (*6*, *35*; PDB codes 2TPS, 1G4E, 1G4P, 1G4S, 1G4T, 1G67, 1G69, and 1G6C). A comparison of the TenI and TPS structures from *B. subtilis* shows an rmsd of 1.8 Å for 184 superimposed Cα atoms (Figure 9). The *tenI* gene has been identified in bacilli, clostridiae, members of the CFB (cytophagea/flavobacter/bacteriodes) group, *Campylobacter jejuni*, *Fusobacterium nucleatum*, *Chlorobium tepidum*, and *Aquifex aeolicus*, and it has been suggested that *tenI* genes are recent paralogues of the gene encoding TPS (*thiE*) (*5*). TenI is frequently misannotated as TPS in many of the gene databanks. A key amino acid substitution at residue 119 in *B. subtilis* TenI of Leu for Gly distinguishes TenI from TPS. This substitution prevents the binding of substrates in the geometry required for the synthesis of thiamin-P.

The structural comparison also reveals that TenI lacks the additional helix α0, which caps the N-terminal barrel entrance of TPS. Other significant structural changes are found in the loop regions that form the active-site pocket in TPS. The active site of TPS is in a pocket formed primarily by the loop regions on the C-terminal end of the barrel: residues 59−67 (A loop, joining β2 and α2), 109−114 (B loop, joining β4 and α4), and 151−168 (C loop, joining β6 and α6). The A loop exists in an altered conformation, the B loop is three amino acid residues longer in TPS, and the C loop is disordered in TenI (Figure 4). The α2 helix, which is involved in the TPS dimer interface, is rotated out from the barrel axis at the C-terminal end by approximately 10° in the TenI structure.

Comparison of the Dimer Interfaces of TenI and TPS. Both TenI and TPS exist as dimers of $(\alpha\beta)_8$ barrels in the crystal structures. The barrels of the TenI dimer are approximately cis to each other (Figure 4). In contrast, the barrel axes of the TPS dimer are arranged in trans orientation with the primary interactions coming from two symmetry-related α2 helices, which are aligned antiparallel to each other along the dimer interface. Native gel results indicate that TenI is most likely a dimer in solution (results not shown), whereas the TPS dimer may be an artifact of crystallization (*6*).

TPS Pyrophosphate and Magnesium Binding Site. In TPS, a pyrophosphate ion is located near the A, B, and C loops, close to the opening of the active site. The binding of pyrophosphate is stabilized by electrostatic and hydrogen-bonding interactions with Arg59 (Arg33), Lys61 (Arg35), Lys159 (Lys129), Ser130 (Ser100), Asn92 (Asn62), six water molecules, and a magnesium atom (TenI structural equivalents are shown in parentheses). The magnesium ion was located on the edge of the active site of TPS. The magnesium ion is coordinated by two aspartate side chains (Asp93 and Asp112), two oxygen atoms from pyrophosphate, and two water molecules. In the TenI structure the two aspartate residues have been replaced with Gly63 and Ser82, thus removing the magnesium binding site. In addition, a proline residue (Pro79) in TenI occupies the approximate position of the magnesium ion found in the TPS structure. Thus, while TenI is structurally homologous to TPS, it is unable to bind the metal ion necessary for stabilization of the pyrophosphate.

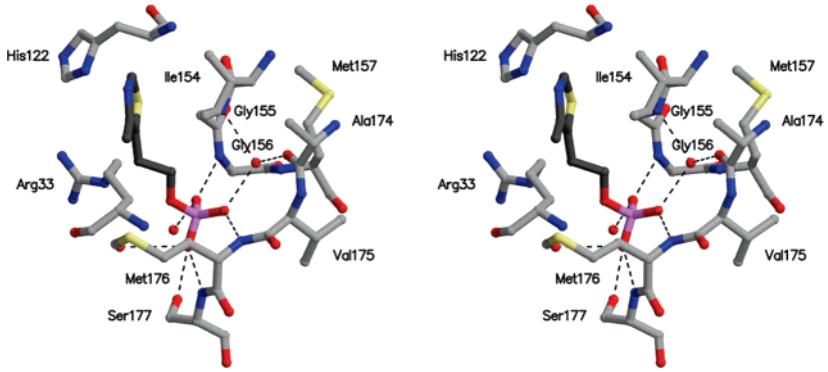

FIGURE 10: Stereodiagram of the thiazole phosphate modeled into the C-terminal end of the TenI barrel. The TenI residues are shown in ball-and-stick representations with the atoms colored according to the scheme described for Figure 3. The carbon atoms of Thz-P are highlighted in dark gray.

These structural changes strongly suggest that TenI is unable to bind HMP-PP.

TPS Thiamin Phosphate Binding Site. The thiamin-P molecule is bound in a V conformation in the TPS enzyme (*6*, *35*). This unique binding conformation is maintained primarily by van der Waals interactions between Ile186 (Ile154) and the pyrimidine and thiazolium rings. The pyrimidine moiety is located at the entrance to the hydrophobic core of the barrel, in a hydrophobic pocket formed by Tyr29 (His4), His107 (Gln77), Tyr147 (Tyr117), Ile186 (Ile154), and Ile208 (Met176). It is hydrogen-bonded to Gln57 (His31) and packs against the imidazole ring of His107 (Gln77). The phosphate moiety of thiamin-P is stabilized by hydrogen-bonding interactions with Thr156 (Thr126, disordered), Thr158 (Cys128), Gly188 (Gly156), Ile208 (Met176), Ser209 (Ser177), and three water molecules. The side chain of Lys159 (Lys129) runs parallel to the thiazolium ethyl group. From the structural superposition of TPS and TenI, a steric clash is observed between Leu119 and the pyrimidine ring of thiamin-P. A sulfate ion was, however, found in the TenI structure in the same position as the phosphate moiety of thiamin-P. The residues involved in forming interactions with the thiazole moiety of thiamin-P are also mostly conserved in the TenI structure. On the basis of the position of the sulfate ion and the structural superposition with the TPS structure, Thz-P was modeled into the TenI structure (Figure 10). All attempts to obtain crystals of a complex of TenI with Thz-P were unsuccessful, likely due to the high sulfate ion concentrations in the crystallization conditions. It is clear, however, that the substitution of Leu for Gly at residue 119 prevents thiamin-P from binding in the same conformation as in TPS, and it appears that TenI is only capable of binding the thiamin-P precursor Thz-P.

Biological Function of TenA/TenI. While the chemical reaction catalyzed by thiaminases I and II is now well defined, the biological function of these enzymes is not yet clear. Thiaminase I occurs in very few bacteria and its gene is never clustered with thiamin biosynthetic genes. The enzyme is secreted into the growth medium where it degrades thiamin. It may play a role in killing competing microorganisms or in the salvage of the thiazole moiety. Thiaminase I has been implicated in the early mortality syndrome in lake salmon, where the ingestion of the thiaminase I-containing alewife by the salmon induces a thiamin deficiency that results in reproductive failure (*36*). Comparative genome analysis demonstrates that the TenA/TenI genes are usually associated with thiamin biosynthetic genes. For example, in *B. subtilis*, TenA/TenI are part of the thiazole biosynthetic operon (TenA−TenI−ThiO−ThiS−ThiG−ThiF−ThiD) and both genes are strongly repressed by thiamin (*2*). This suggests that TenA/TenI are involved in some aspect of thiamin biosynthesis or metabolism.

The transition between exponential growth and stationary phase in bacteria is characterized by the secretion of degradative enzymes such as proteases and glycosidases. In *B. subtilis*, gene expression during this phase is modulated by a class of proteins known as the Deg proteins (*4*). Mutations in these proteins affect the production of the degradative enzymes produced during the transition phase. These mutations also lead to changes in the development of competence, synthesis of flagella, and in sporulation. There is evidence of a relationship between TenA and TenI and the Deg proteins, in that the overexpression of TenA in *B. subtilis* results in an increase in the secretion of the degradative enzymes subtilisin, neutral protease, and levansucrase, and the presence of TenI attenuates this activity 5-fold (*3*). DegS, one of the proteins in the Deg system, undergoes autophosphorylation in response to an unknown signal. It is tempting to speculate that this unknown signal may in some way be due to the binding and/or degradation of thiamin by TenA. If so, this would be an exciting example of the use of a vitamin in cell signaling.

ACKNOWLEDGMENT

We thank NE-CAT beam line 8-BM, supported by NIH Grant RR15301, and the Cornell High Energy Synchrotron Source for provision of beam time. NIH Grant R01DK044083 (T.P.B.) provided support for this project. We thank Dr. Cynthia Kinsland for the preparation of the TenA overexpression plasmid and mutants, and Leslie Kinsland for assistance in the preparation of this manuscript.

REFERENCES

1. Settembre, E., Begley, T. P., and Ealick, S. E. (2003) Structural biology of enzymes of the thiamin biosynthesis pathway, *Curr. Opin. Struct. Biol. 13*, 739−747.
2. Lee, J.-M., Zhang, S., Saha, S., Santa Anna, S., Jiang, C., and Perkins, J. (2001) RNA expression analysis using an antisense *Bacillus subtilis* genome array, *J. Bacteriol. 183*, 7371−7380.
3. Pang, A. S. H., Nathoo, S., and Wong, S. L. (1991) Cloning and characterization of a pair of novel genes that regulate production of extracellular enzymes in *Bacillus subtilis*, *J. Bacteriol. 173*, 46−54.
4. Strauch, M. A. (1993) Regulation of *Bacillus subtilis* gene expression during the transition from exponential growth to stationary phase, *Prog. Nucleic Acid Res. Mol. Biol. 46*, 121−53.
5. Rodionov, D. A., Vitreschak, A. G., Mironov, A. A., and Gelfand, M. S. (2002) Comparative Genomics of Thiamin Biosynthesis in Procaryotes. New genes and regulatory mechanisms, *J. Biol. Chem. 277*, 48949−48959.
6. Chiu, H., Reddick, J., Begley, T., and Ealick, S. (1999) Crystal structure of thiamin phosphate synthase from *Bacillus subtilis* at 1.25 Å resolution, *Biochemistry 38*, 6460−6470.
7. Bradford, M. M. (1976) A rapid and sensitive method for the quantitation of microgram quantities of protein utilizing the principle of protein−dye binding, *Anal. Biochem. 72*, 248−54.
8. Jancarik, J., and Kim, S. H. (1991) Sparse-Matrix Sampling−a Screening Method for Crystallization of Proteins, *J. Appl. Crystallogr. 24*, 409−411.
9. Otwinowski, Z., and Minor, W. (1997) Processing of X-ray diffraction data collected in oscillation mode, *Methods Enzymol. 276*, 307−326.
10. Itou, H., Yao, M., Watanabe, N., and Tanaka, I. (2004) Structure analysis of PH1161 protein, a transcriptional activator TenA homologue from the hyperthermophilic archaeon *Pyrococcus horikoshii*, *Acta Crystallogr. D 60*, 1094−1100.
11. Sali, A., and Blundell, T. L. (1993) Comparative protein modelling by satisfaction of spatial restraints, *J. Mol. Biol. 234*, 779−815.
12. Marti-Renom, M. A., Yerkovich, B., and Sali, A. (2002) *Comparative protein structure prediction*, Wiley, New York.
13. Vagin, A., and Teplyakov, A. (2000) An approach to multi-copy search in molecular replacement, *Acta Crystallogr. D 56*, 1622−4.
14. Collaborative Computational Project Number 4. (1994) The CCP-4 suite: programs for protein crystallography, *Acta Crystallogr. D 50*, 760−763.
15. Jones, T. A., Zou, J.-Y., Cowan, S. W., and Kjeldgaard, M. (1991) Improved methods for the building of protein models in electron density maps and the location of errors in these models, *Acta Crystallogr. A 47*, 110−119.
16. Brünger, A. T., Adams, P. D., Clore, G. M., DeLano, W. L., Gros, P., Grosse-Kunstleve, R. W., Jiang, J. S., Kuszewski, J., Nilges, M., Pannu, N. S., Read, R. J., Rice, L. M., Simonson, T., and Warren, G. L. (1998) Crystallography & NMR system: A new

software suite for macromolecular structure determination, *Acta Crystallogr. D 54*, 905−21.
17. Esnouf, R. (1997) An extensively modified version of Molscript which includes greatly enhanced colouring capabilities, *J. Mol. Graphics 15*, 132−134.
18. Esnouf, R. M. (1999) Further additions to MolScript version 1.4, including reading and contouring of electron-density maps, *Acta Crystallogr. D 55*, 938−40.
19. Merritt, E. A. and Bacon, D. J. (1997) Raster3D: Photorealistic Molecular Graphics, *Methods Enzymol. 277*, 505−524.
20. Christopher, J. A. (1998) SPOCK, Texas A&M University, College Station, TX.
21. Miller, R., DeTitta, G. T., Jones, R., Langs, D. A., Weeks, C. M., and Hauptman, H. A. (1993) On the application of the minimal principle to solve unknown structures, *Science 259*, 1430−3.
22. Miller, R., Gallo, S. M., Khalak, H. G., and Weeks, C. M. (1994) SnB: crystal structure determination via shake-and-bake, *J. Appl. Crystallogr. 27*, 613−21.
23. Smith, G. D., Nagar, B., Rini, J. M., Hauptman, H. A., and Blessing, R. H. (1998) The use of SnB to determine an anomalous scattering substructure, *Acta Crystallogr. D 54*, 799−804.
24. Laskowski, R. A., MacArthur, M. W., Moss, D. S., and Thornton, J. M. (1993) PROCHECK: a program to check the stereochemical quality of protein structures, *J. Appl. Crystallogr. 26*, 283−291.
25. Ramakrishnan, C. and Ramachandran, G. N. (1965) Stereochemical criteria for polypeptide and protein chain conformations. II. Allowed conformations for a pair of peptide units, *Biophys. J. 5*, 909−33.
26. Holm, L.. and Sander, C. (1993) Protein structure comparison by alignment of distance matrixes, *J. Mol. Biol. 233*, 123−38.
27. Evans, W. C. (1975) Thiaminases and their effects on animals, *Vitam. Horm. 33*, 467−504.
28. Fujita, A. (1954) Thiaminase, *Adv. Enzymol. 15*, 389−421.
29. Costello, C. A., Kelleher, N. L., Abe, M., McLafferty, F. W., and Begley, T. P. (1996) Mechanistic studies on thiaminase I. Overexpression and identification of the active site nucleophile, *J. Biol. Chem. 271*, 3445−52.
30. Campobasso, N., Costello, C., Kinsland, C., and Begley, T. P. (1998) Crystal structure of thiaminase I from *Bacillus thiaminolyticus* at 2.0 Å resolution, *Biochemistry 37*, 15891−15989.
31. Lienhard, G. E. (1970) Kinetic evidence for a (4-amino-2-methyl-5-pyrimidinyl)methyl-enzyme intermediate in the thiaminase I reaction, *Biochemistry 9*, 3011−20.
32. Nicewonger, R., Costello, C. A., and Begley, T. P. (1996) Mechanistic Studies on Thiaminase I. 3. Stereochemistry of the Thiaminase I and the Bisulfite-Catalyzed Degradation of Chiral Monodeuteriothiamin, *J. Org. Chem. 61*, 4172−4174.
33. Zoltewicz, J. A., Uray, G., and Kauffman, G. M. (1980) Evidence for an Intermediate in Nucleophilic-Substitution of a Thiamin Analogue−Change from 1st-Order to 2nd-Order Kinetics in Sulfite Ion, *J. Am. Chem. Soc. 102*, 3653−3654.
34. Larsen, T. M., Benning, M. M., Rayment, I., and Reed, G. H. (1998) Structure of the bis(Mg^{2+})−ATP−oxalate complex of the rabbit muscle pyruvate kinase at 2.1 Å resolution: ATP binding over a barrel, *Biochemistry 37*, 6247−55.
35. Peapus, D., Chiu, H.-J., Campobasso, N., Reddick, J., Begley, T., and Ealick, S. (2001) Structural characterization of the enzyme−substrate, enzyme-intermediate, and enzyme−product complexes of thiamin phosphate synthase, *Biochemistry 40*, 10103−10114.
36. Fisher, J. P., Fitzsimons, J. D., Combs, G. F., Jr., and Spitsbergen, J. M. (1996) Naturally occurring thiamine deficiency causing reproductive failure in finger lakes atlantic salmon and great lakes lake trout, *Trans. Am. Fish. Soc. 125*, 167−78.

BI0478648